Theoretical studies of defect states in GaTe

2009 J. Phys.: Condens. Matter 21 015504

(http://iopscience.iop.org/0953-8984/21/1/015504)

J. Phys.: Condens. Matter **21** (2009) 015504 (9pp) doi:10.1088/0953-8984/21/1/015504

Theoretical studies of defect states in GaTe

Zs Rak[1], S D Mahanti[1,4], Krishna C Mandal[2] and Nils C Fernelius[3]

[1] Department of Physics and Astronomy, Michigan State University, East Lansing, MI 48824, USA
[2] EIC Laboratories, Incorporated, 111 Downey Street, Norwood, MA 02062, USA
[3] AFRL/RX, WPAFB, OH 45433, USA

E-mail: mahanti@pa.msu.edu

Received 29 July 2008, in final form 30 October 2008
Published 1 December 2008
Online at stacks.iop.org/JPhysCM/21/015504

Abstract

Using first principle electronic structure calculations within density functional theory and the supercell model, we have investigated the nature and formation energies of defect states associated with Ga and Te vacancies and Ge and Sn substitutional impurities in GaTe. We have also calculated the band structure of pure GaTe for comparison with systems with defects and also to find out the importance of spin–orbit interaction (SOI) on its band structure. We find that the top valence band at the Γ-point shifts up in energy by ∼0.1 eV due to the mixing of Te p_x–p_y and p_z bands, this splitting being considerably smaller than in atoms where it is ∼0.8 eV. From an analysis of charge densities and band structures associated with the defect states, we find that most of them are strongly localized and lie deep in the band gap region. The calculated binding energy of the deep defect state and the $\varepsilon(-1/-2)$ transition level associated with the Ga vacancy appears to be in good agreement with experiment. Formation energy calculations suggest that V_{Ga} is the preferred intrinsic defect in GaTe.

(Some figures in this article are in colour only in the electronic version)

1. Introduction

The family of III–VI semiconductors, such as GaS, GaSe, GaTe and InSe has been extensively studied due to their nonlinear optical properties [1] and their possible application in optical devices [2, 3]. They crystallize in a layered structure, each layer being composed of four monoatomic anion–cation–cation–anion layers. As a result, their optical and transport properties are highly anisotropic. One of the main characteristics of the III–VI systems is the presence of cation–cation dimers oriented perpendicular to the layers. GaTe occupies a special place among the members of the III–VI family, since its crystal structure is more complex compared to the other members [4]. In this compound there are Te–Ga–Ga–Te layers and Ga–Ga dimers, similar to the rest of the group, but only two-thirds of these dimers are oriented perpendicular to the layers, while for the remaining one-third the Ga–Ga bonds lie almost in the layer plane (figure 1). GaTe belongs to the $B2/m$ space group and crystallizes in the monoclinic system [5]. Although the overall crystal structure of GaTe appears to be more complicated than GaSe, the local coordination of the atoms is similar to that of the other III–VI compounds: each Ga atom is fourfold coordinated to three Te and one Ga atom, while each Te atom is threefold coordinated to three Ga atoms. The bonds within the layers have a strong covalent character while the layers are bound mainly by a weak van der Waals type interaction. Unlike GaS, GaSe and InSe, no polytypism has been observed in GaTe [6, 7]. Whether this has to do with the presence and orientation of Ga–Ga (In–In) dimers in the layer is not known at the present time.

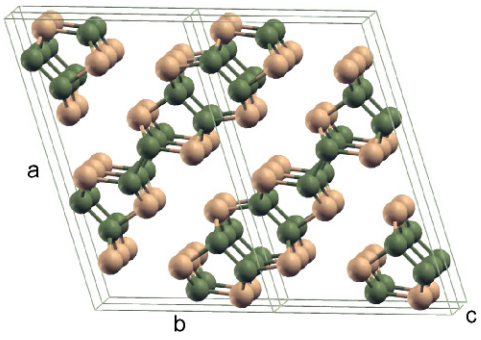

Figure 1. The crystal structure of GaTe. Dark spheres are the Ga atoms and the light spheres are Te atoms. In each layer one can see the Ga–Ga dimers; two oriented normal to the layer and one oriented along the layer.

[4] Author to whom any correspondence should be addressed.

Experimental investigations in GaTe have focused on the structural, optical, and photo emission properties associated with its layered structure [8–13]. Schwartz *et al* [14] have observed that GaTe undergoes a structural phase transition at 10 GPa into a metallic NaCl-type structure. Pellicer-Porres *et al* [15] used x-ray absorption spectroscopy to study the evolution of the bond lengths in GaTe under pressure. The same authors [16] observed a nonlinear pressure dependence of the direct band gap in their optical absorption measurements. Extensive transport measurements have been carried out in p-type GaTe by Efeoğlu *et al* [17]. Experiments dealing specifically with defect energy levels will be discussed along with our theoretical calculations.

Because of its more complex structure, there is a lack of detailed theoretical investigation of the electronic properties of GaTe. Yamamoto *et al* [6] calculated the electronic structure of GaTe using the *ab initio* tight-binding linear muffin-tin orbitals (TB-LMTO) method within the atomic sphere approximation (ASA). For the exchange and correlation potential they have used the *von Barth–Hedin* local density approximation (LDA). From a comparison of their theoretical band structure to optical absorption spectra they concluded that the dominant excitations were associated with $j-j$ coupled, optically allowed exciton states. A more detailed analysis of the GaTe band structure was done by Sánchez-Royo *et al* [8], using numerical atomic orbitals and density functional theory (NAO-DFT), in the local density approximation.

The dispersion of the valence bands along different directions in the Brillouin zone (BZ) was compared with angle-resolved photoemission spectroscopy (APRES) measurement. Although there were qualitative agreements between theory and experiment as regards band dispersion, there were major differences. To explain these differences Sánchez-Royo *et al* [8] suggested that the spin–orbit interaction (SOI) increased the mixing between the Te p_z states from the top of the valence band (VB) and the deeper Te p_x, p_y states, leading to an upward shift and flattening of the topmost VB near the Γ-point. We have checked this suggestion by carrying out explicit calculations and discuss the results later in this paper.

In general, the electronic transport and dominant optical properties of a semiconductor are determined mainly by the electronic states near the band gap region. These states are easily influenced by the defects present in the system. The defects therefore play an important role in the performance of a semiconductor. In this paper we have investigated the nature of the defect states in GaTe associated with native point defects (Ga and Te vacancies) and substitutional impurities (Ge and Sn on Ga site) within *ab initio* density functional theory (DFT) using the generalized gradient approximation (GGA). The defects are put in large super cells to minimize defect–defect interaction. It is well known that due to the underestimation of the band gap by LDA or GGA and due to the limitations of the supercell model [18], accurate calculation of the defect energy levels represents a serious theoretical challenge, particularly when they are formed out of conduction band states (donor states) or they overlap with the conduction band (deep defect states overlapping the conduction band). However, in the case of acceptor states, derived mostly from the valence band, their position relative to the valence band maximum (VBM) can be obtained with reasonable accuracy using supercell models provided proper corrections are made to take care of the effect of the defects on the host valence band structure. In this work we have estimated the energy of the defect levels when these are derived mainly from the valence band or when they are deep defect states lying in the band gap. We have also calculated the formation energies of defects in different charge states and discuss the dependence of the formation energies on the chemical potentials of the constituent elements under equilibrium growth conditions.

The arrangement of the paper is as follows. In section 2 we describe the GaTe supercell and the methods used to perform the structural optimization and electronic structure calculation. Section 3 is divided into four subsections: results for pure GaTe, electronic structure of Ga and Te vacancies, electronic structure of substitutional impurities and study of the defect formation energies and charge transition levels. A brief summary is given in section 4.

2. Computational details

We have performed structural optimizations and electronic structure calculations using projector augmented wave (PAW) [19] methods implemented through the VASP [20] package. The exchange and correlation potential was approximated by the generalized gradient approximation (GGA) [21]. The 3d, 4s and 4p states of Ga and 5s and 5p states of Te were treated as valence states and the rest as cores. The energy cutoff was set to 300 eV and convergence was assumed, when the energy difference between consecutive cycles was less than 10^{-4} eV. The internal structural parameters of pure and defect containing GaTe were optimized using the conjugate gradient algorithm [22]. The convergence criterion for atomic relaxation was set to a 10^{-3} eV energy difference between two consecutive ionic relaxation steps.

For the structure optimization and total energy calculation of pure GaTe, we have used the conventional unit cell containing 12 Ga and 12 Te atoms. The Brillouin zone (BZ) was sampled by a Γ-centered Monkhorst–Pack [23] grid of $2 \times 4 \times 10$ k-points ($36k$ points in the irreducible (IBZ)). To model Sn and Ge substitutional defects in GaTe, we have constructed $1 \times 2 \times 4$ supercells (192 atoms) starting from the conventional unit cell and replaced one Ga atom by either Sn or Ge. Supercells of the same size were used to simulate the intrinsic defects (such as Ga and Te vacancies) in GaTe. These calculations were performed using $3 \times 3 \times 3$ Γ-centered Monkhorst–Pack k-meshes. In order to reduce the spurious defect–defect elastic interactions within neighboring supercells, the calculations were performed using the theoretical lattice constants of the bulk GaTe, as suggested in [24].

To check the accuracy of our calculations obtained with the PAW method we have compared the band structures of pure GaTe with that obtained using the full potential linearized augmented plane wave (FPLAPW) [25] method, implemented through the Wien2k [26] package. For the full potential calculation we used the following setup: the 3d, 4s, 4p

Table 1. The experimental and theoretical lattice parameters of bulk GaTe. The distances are given in angstroms and the monoclinic angle γ in degrees. $d^{\perp}_{\mathrm{Ga-Ga}}$ and $d^{\parallel}_{\mathrm{Ga-Ga}}$ refer to the Ga–Ga dimer lengths that are perpendicular and parallel to the layer planes, respectively.

	a	b	c	γ	$d^{\perp}_{\mathrm{Ga-Ga}}$	$d^{\parallel}_{\mathrm{Ga-Ga}}$
Exp. [30]	17.44	10.46	4.08	104.4	2.43	2.44
Theor.	18.56	10.96	4.14	107.6	2.46	2.49

electrons of Ga and 4d, 5s, 5p electrons of Te were treated as valence electrons, the product between the smallest muffin-tin radius (R_{MT}) and the largest reciprocal lattice vector (K_{max}) were chosen such that $R_{\mathrm{MT}}K_{\mathrm{max}} = 7.0$. The atomic radii were 2.17 a.u. for Ga and 2.35 a.u. for Te and convergence was assumed when the energy difference between the self-consistent cycles was less than 0.0001 Ryd (1.36 meV). The small differences in the results obtained by the two methods are related primarily to the volume relaxation and structure optimization. The electronic band structures and the density of states, however, are nearly identical, as expected. Thus, all the results given in this paper are obtained with the PAW method except for the band structure of pure GaTe (which was calculated using both the PAW and FPLAPW methods). To verify whether the large effect of SOI on the band structure suggested in [8] is reasonable, we have calculated and compared the electronic structures of bulk GaTe with and without SOI using FPLAPW. We find SOI effects on the band structure to be quite small and therefore have not included it in our defect containing supercell calculations.

3. Results

3.1. Pure GaTe

To relax the structure of bulk GaTe (figure 1), using the PAW method, first we performed volume optimization keeping the ratio of the lattice parameters a:b:c constant and then minimized the internal structural parameters at constant volume allowing the shape of the cell to change. The initial a:b:c ratio was chosen based on the values of the experimental lattice constants [30], and it was allowed to change when the internal parameters were varied. The obtained lattice parameters a, b, and c are larger than the experimental ones by 6.4%, 4.7% and 1.5% respectively. The large overestimation of the lattice constants a and b can be attributed to the underbinding effect of GGA, which is enhanced by the weak Van der Waals interlayer interaction along the a- and b-axis. Since the crystal c-axis lies in the plane of the GaTe layers (and the intralayer interaction is a strong, covalent type), the effect of overestimation of the lattice constants by GGA is less evident on the c-axis. After this two-step relaxation process we have performed one more volume optimization to check if the calculated lattice constants are close to their optimal values. Since the lattice parameters after the additional volume optimization increased by only ∼0.01 Å, we considered that the crystal structure obtained after the initial two-step process is close enough to the fully relaxed structure. The theoretical lattice constants and the relaxed Ga–Ga dimer lengths are given in table 1.

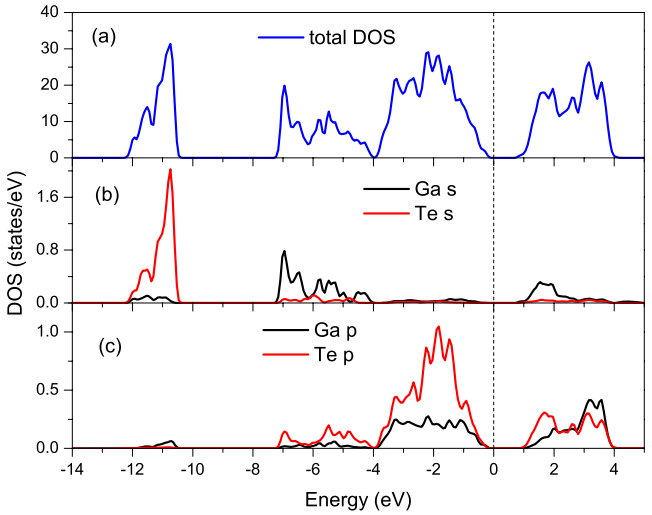

Figure 2. (a) Total density of states (DOS) of the gate crystal calculated using the PAW method; (b) and (c) projected DOS of s and p orbitals respectively of Ga and Te.

In figure 2 we show the total density of states (DOS) of GaTe calculated with the PAW method along with the partial DOS of Ga and Te. The origin of the energy was chosen at the highest occupied level. The valence band of GaTe can be divided into three main groups. The first group of peaks located between −12.5 and −10.5 eV originates mainly from Te 5s states with a very small Ga 4s and 4p contribution. The second group of bands, from −7.2 to −4.0 eV displays a pronounced Ga 4s character with a significant contribution from the Te 5p states. The highest group of bands from −4.0 to 0 eV (energy of the highest occupied state) is formed by a strong hybridization of Te 5p and Ga 4p states. The bottom of the conduction band is a mixture of almost equal contributions from Te 5p and Ga 4s, with a smaller Ga p character.

By looking at the electronic band structure of bulk GaTe, obtained by the FPLAPW method using the primitive unit cell (6 Ga and 6 Te atoms) and with SOI included (figure 3), we can identify the three main groups of valence bands mentioned in the previous paragraph: (i) the lowest group of 6 bands (Te 5s) is split off from the upper part of the valence band by approximately 3.0 eV; (ii) the next 6 bands, with strong Ga 4s character, correspond to Ga–Ga bonding and antibonding states associated with the Ga–Ga dimers; (iii) the upper 15 bands originate from Te 5p states (15 out of 18 Te p states associated with 6 Te atoms/unit cell) hybridized with Ga 4p states. The electron counting is such that the 6 Ga s and the 6 Te s bands together with the 15 hybridized Te–Ga p bands can accommodate the total number of 54 valence electrons (18 from Ga and 36 from Te). Therefore 3 Te 5p states (out of 18) remain empty and are pushed up in energy giving rise to a semiconducting gap in the band structure of GaTe. If we look at the dispersion of the Ga s bands we see one bonding band is quite flat compared to the other two. It is also present to some extent for the antibonding s bands. This asymmetry is a result of the structure where two of the three Ga dimers are oriented differently compared to the third one.

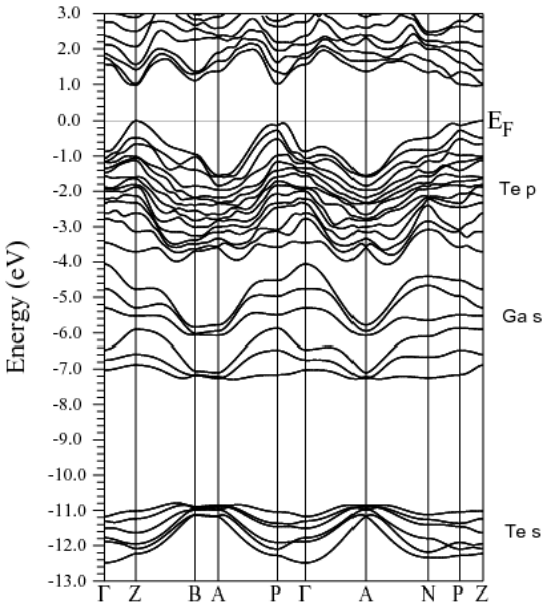

Figure 3. Band structure of the GaTe crystal along the high symmetry directions, calculated using the FPLAPW method. The Brillouin zone used in this calculation is identical to the one described in [8].

The overall shapes of the electronic DOS and band structure calculated by the PAW and FPLAPW methods are similar to those obtained previously by tight-binding (TB-LMTO) [6] and pseudo-potential (NAO-DFT) [8] approaches. Small differences in the orbital contributions to the DOS, however, exist throughout the valence band. This is understandable since all the calculations were done within LDA/GGA. According to our calculation the Ga s contribution to the low-energy valence bands (-12.5 to -10.5 eV) is stronger than the Ga p contribution, in contrast with the results reported by Sanchez-Royo *et al* [8], where the Ga p character was found to be stronger than the Ga s. Also the contribution of Te s and Te p to the DOS in the region -7.2 to -6.0 eV is about the same order in our calculations, whereas in [6] the Te p character is much more pronounced. The quasi-gap in the valence band at about ∼4 eV was also present in the TB-LMTO calculation of Yamamoto *et al* [6] and it is in agreement with the ultraviolet photoelectron spectroscopy (UPS) measurement [27].

In order to understand the effect of SOI in GaTe we plot in figure 4 the calculated band structures along the Γ–Z direction (*a*) without SOI and (*b*) with SOI. As seen in the figure, the most significant effect is the energy shift-up of the top valence bands at the Γ-point when SOI is included in the calculation. This effect is explained well by Sanchez-Royo *et al* [8]; the bands with p_x–p_y character, which lie below the topmost VB, split under spin–orbit interaction and those with $j = 3/2$ shift up in energy. However, the magnitude of the energy shift calculated with the FPLAPW method (∼0.1 eV) is much less than the energy shift estimated in [8] (0.7–0.9 eV) inferred from the atomic data. Thus in solids where the Te orbitals are much more diffuse SOI effects are quite small. The effect of SOI on the energy position of the Te bands has been calculated in PbTe [28], and a similar value of ∼0.1 eV was obtained. The above analysis clearly suggests that the SOI in GaTe is rather small, as it is in the other members of the III–VI family [29].

From our band structure calculations we see that GaTe is a direct gap semiconductor with the gap located at the Z point, at the edge of the BZ, in agreement with the previous theoretical results [6, 8]. Our band gap of 0.98 eV (and 1.098 eV obtained in [8]) is underestimated by a factor of almost two compared to the experimental value of 1.799 eV [30], due to the well-known limitation of LDA (GGA), which underestimates the band gap in semiconductors [31].

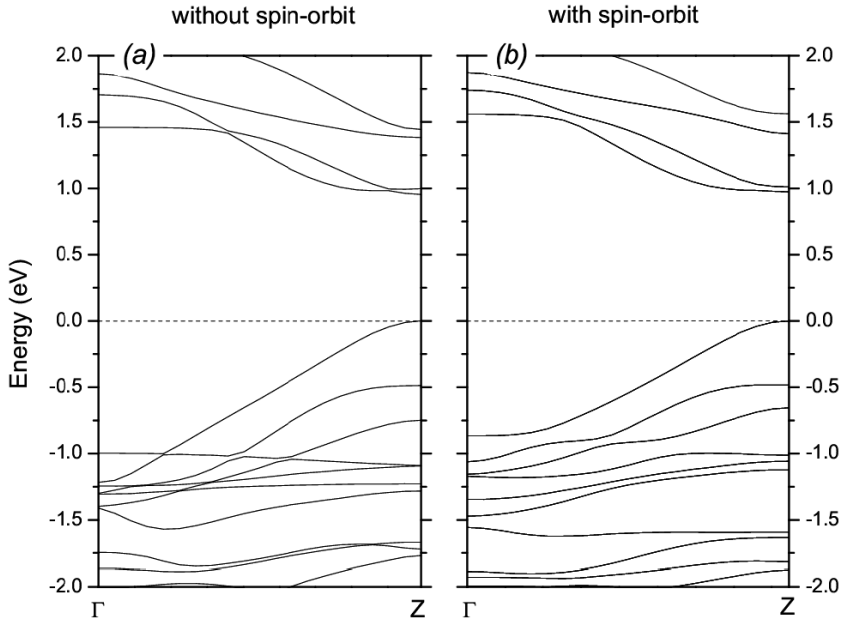

Figure 4. Band structure of GaTe (*a*) without and (*b*) with spin–orbit interaction. The bands with p_x–p_y character, which lie below the topmost VB, split under spin–orbit interaction and those with $j = 3/2$ shift up in energy by ∼0.1 eV.

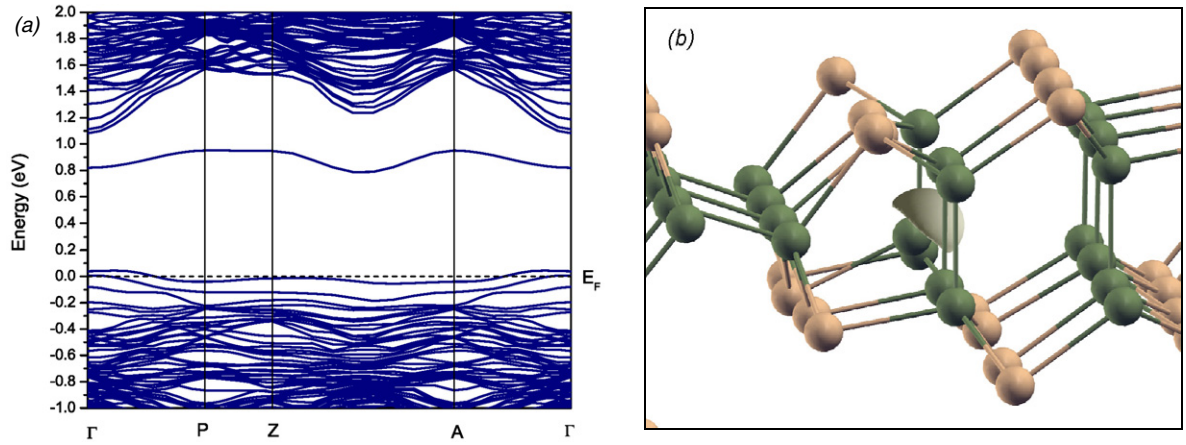

Figure 5. (*a*) The band structure of GaTe with a Ga vacancy. (*b*) The charge density associated with the vacancy induced deep defect band (lying in the gap near energy 0.8 eV).

3.2. Vacancies in GaTe

For the vacancy calculations we minimize the energy of the $1 \times 2 \times 4$ supercell containing one Ga vacancy (V_{Ga}) or one Te vacancy (V_{Te}). For V_{Ga}, the supercell contains 96 Te, 95 Ga, and a vacant Ga site. The shortest distance between two vacancies is 16.56 Å. After the optimization of the atomic positions we observe a large inward relaxation of the atoms that are nearest neighbors (NN) of the vacancy. There are significant changes in the bond lengths and bond angles. To quantify this inward atomic relaxation we give, in table 2, distances between the vacancy and the Ga and Te atoms surrounding the vacancy. For comparison we also give the corresponding bond lengths for pure GaTe inside parenthesis. The vacancies are considered to be at the ideal atomic positions.

To understand the nature of the defect states introduced by the vacancies in GaTe, we have calculated the electronic band structure of the defect containing supercells and the charge densities associated with the defect induced bands. Introducing a Ga vacancy means that there is one less Ga s state in the VB and three less electrons in the system. Thus, for one Ga atom removed, we expect partially filled bands near the top of the VB. From the band structure plot in figure 5(*a*) we see that there is indeed one partially filled band crossing the E_F along the Γ–P and A–Γ directions. Besides this, a Ga vacancy introduces a narrow defect band lying deep in the gap region. The energy of this deep defect state with respect to the VBM of the vacancy containing supercell (which occurs at the Γ point) is ∼0.78 eV. This value is consistent with the hole trapping level measured by deep-level transient spectroscopy at 0.8 eV above the VB by Sighetomi *et al* [32]. Manfredotti *et al* [33] also report an acceptor level at 0.74 eV above VB in melt grown samples of GaTe. It is tempting to presume that this defect level originates from the Ga vacancy. One should however note that in experiments the defect concentrations are much smaller than we have in our supercell calculations. Consequently one must correct for the changes in the VBM energy. To estimate these corrections we match the energies of the Ga 3d semicore states of the pure and vacancy containing GaTe, at Γ-point. We find that the energy of the defect level with respect to the VBM of the pure GaTe shifts to ∼0.82 eV. This value is still in good agreement with the experiment, suggesting that the defect level might indeed come from Ga vacancy. Figure 5(*b*) shows the electronic charge density associated with this deep defect band. The charge density originates mainly from Ga s states in the vicinity of the vacancy and it is highly localized.

Table 2. The distances between the vacancies and their nearest neighbors. The notations of Ga1 and Ga2 refer to the Ga atoms from the dimers oriented perpendicular and parallel to the atomic layers, respectively. The bond lengths of the pure GaTe are given in parenthesis. The distances are given in angstroms.

	Gallium vacancy	Tellurium vacancy
Vacancy-Ga1	1.87 (2.46)	2.27 (2.73)
Vacancy-Ga2		2.59 (2.71)
Vacancy-Te	2.23 (2.71)	4.07 (4.19)
Te–Te	3.64 (4.19)	

For V_{Te} we find that the band structure also changes drastically (see figure 6(*a*)) compared to pure GaTe. The changes in the band structure introduced by a Te vacancy can be qualitatively understood in terms of the bonding model described in the case of GaSe [34] since the local bonding between Ga and Te is similar to that between Ga and Se. As discussed earlier, the Ga–Ga dimers form bonding and antibonding states (the six Ga s bands indicated in figure 3). Due to the hybridization between the Ga s states and Te p states, some of the Te bands are pushed up in energy, giving rise to the semiconducting gap. In the case of pure GaTe there are 6 Ga and 6 Te atoms in the unit cell. Three Te p states (out of 18) are pushed up to the CB. Removing one Te atom from the unit cell (Ga_6Te_5) gives rise to one less Te s state and two less Te p states in the VB and one less Te p state in the CB. Since the number of electrons is reduced by 6 due to the Te vacancy we expect that all the valence bands will be fully occupied (no partial occupation). To check this point we counted the number of valence bands obtained in the pure and in the vacancy containing supercells. The number

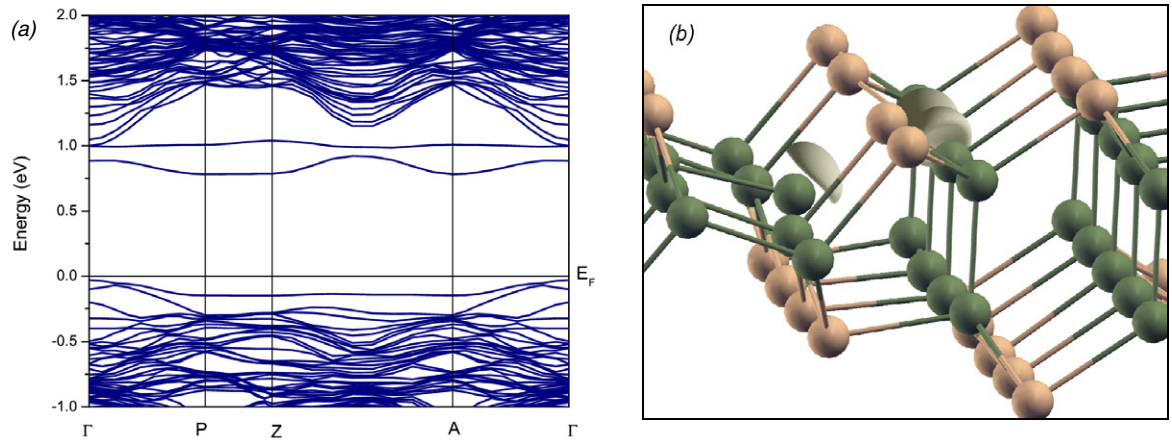

Figure 6. (*a*) The band structure of GaTe with a Te vacancy. (*b*) The charge density associated with the two, vacancy induced deep defect bands which lie below the CB.

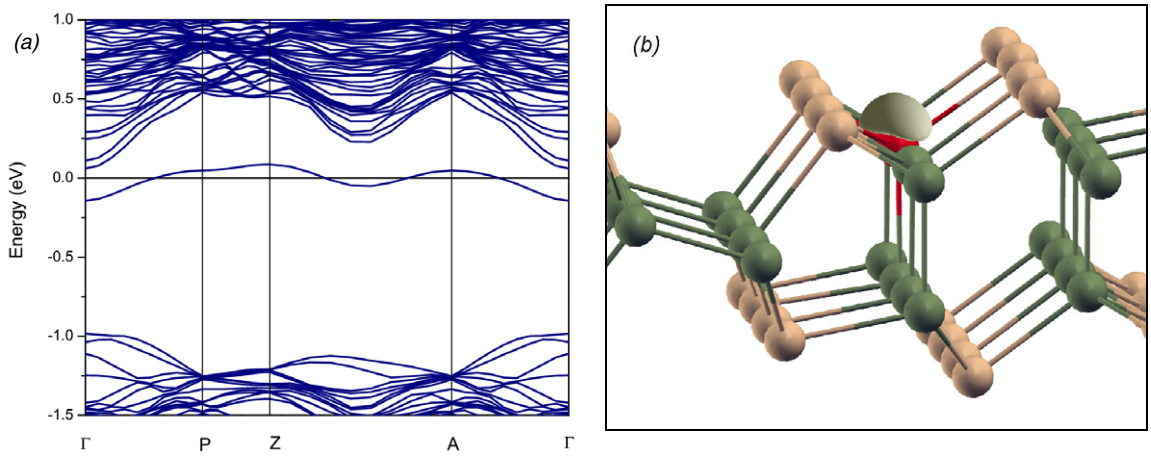

Figure 7. (*a*) The band structure of GaTe doped with Ge (or Sn) on the Ga site. (*b*) The charge density associated with the impurity induced defect band.

of valence bands indeed decreases by three (disregarding spin degeneracy) when one Te atom is removed from the 192-atom system. In figure 6(*a*) we see that Te vacancy introduces two gap states right below the CB and one nearly non-dispersive resonant state near the top of the VB. From the charge density plots associated with the two gap states below the conduction band shown in figure 6(*b*) we see that these bands originate from the p states of Ga atoms surrounding the Te vacancy. A Te vacancy acts like an attractive potential and lowers the energies of the neighboring Ga p states. Doping these two states can give rise to magnetism.

3.3. Ge and Sn substitutional impurities in GaTe

In the case of simple extrinsic impurities, one should be able to predict whether the impurity will give rise to a donor state or acceptor state by simply counting the number of valence electrons of the dopant and the host atoms. The addition of group IV elements, such as Si, Ge, Sn or Pb, to the Ga site, introduces more electrons into the system, giving rise to donor states. Figure 7(*a*) shows the calculated band structure for the Ge impurity. Since Sn behaves very similar to Ge, we only present the results for the latter and point out the noticeable differences between the two.

Table 3. Optimized impurity–host bond lengths. The last row contains the per cent increase in the bond lengths relative to the ones obtained for the bulk GaTe.

	d_{Ge-Ga}	d_{Ge-Te1}	d_{Ge-Te2}	d_{Sn-Ga}	d_{Sn-Te1}	d_{Sn-Te2}
	2.56	2.75	2.74	2.73	2.92	2.90
Increased by (%)	4.5	2.6	1.1	9.8	8.9	7.4

Let us first discuss the local atomic relaxation in the neighborhood of the impurity. Since one of the major differences between Ge and Sn atoms is in their sizes, we observe noticeable differences in the relaxation of the atomic positions around the Ge and Sn defects. In both cases the atoms surrounding the Ge or Sn relax outward, but in the case of the Sn, the relaxation is much stronger. The optimized impurity–host bond lengths are listed in table 3.

Next we look at the position of the defect states. The defect level lies deep in the gap region, closer to the CBM and

it is partially filled. Due to the well-known problem of the underestimation of the band gap by LDA/GGA, the position of this level with respect to the CBM cannot be obtained reliably. However, if we measure their position from the respective VBM, we find that they are about ∼1 eV above the VBM and compared to Sn, the Ge level is closer to the VBM by ∼50 meV. Figure 7(*b*) shows that the charge density associated with the impurity state is strongly localized around the defect and it originates primarily from Ge p orbitals.

3.4. Defect formation energies and charge transition levels

We would now like to discuss the formation energies of different types of defects in GaTe and see how they depend on the atomic chemical potentials. We adopt the formalism described in [35–37]. The formation energy of a defect α in GaTe in charge state q can be written as:

$$\Delta H_{\rm f}(\alpha, q) = \Delta E(\alpha, q) + n_{\rm Ga}\mu_{\rm Ga} + n_{\rm Te}\mu_{\rm Te} + n_\alpha\mu_\alpha + qE_{\rm F}, \tag{1}$$

where

$$\Delta E(\alpha, q) = E(\alpha, q) - E({\rm GaTe}) + n_{\rm Ga}E({\rm Ga}) + n_{\rm Te}E({\rm Te}) + n_\alpha E(\alpha) + qE_{\rm VBM}. \tag{2}$$

In the above equations $E(\alpha, q)$ and E(GaTe) are the total energies of the defect containing and the defect-free supercells and E(i)s (i = Ga, Te, impurity) are the energies of the constituents in their standard solid state. μ_is are the atomic chemical potentials referenced to E(i) and $n_{\rm i}$s are the number of atoms removed from ($n_{\rm i} > 0$) or added to ($n_{\rm i} < 0$) the system. $E_{\rm F}$ represents the electron chemical potential (Fermi energy) referenced to the energy of the VBM ($E_{\rm VBM}$). q is the charge state of the defect. The value of $E_{\rm F}$ where the formation energies of the same defect in different charge states (q and q') are equal defines the charge transition level:

$$\varepsilon(q/q') = [\Delta E(\alpha, q') - \Delta E(\alpha, q)]/(q' - q). \tag{3}$$

Equation (1) shows that by changing the atomic chemical potentials of the constituent elements, one can adjust the defect formation energy and consequently the solubility of the dopants. However, the values achievable by the chemical potentials are limited by several equilibrium growth conditions [35–37]: in order to avoid precipitations of Ga, Te or dopant elements, the μs have to satisfy $\mu_{\rm Ga} \leqslant 0$, $\mu_{\rm Te} \leqslant 0$, $\mu_{\rm dopant} \leqslant 0$; to maintain a thermodynamically stable GaTe host compound, $\mu_{\rm Ga} + \mu_{\rm Te} = H_{\rm f}$(GaTe), where $H_{\rm f}$(GaTe) is the enthalpy of formation of GaTe; and finally, in order to avoid formation of secondary phases between the dopants and the host elements (denoted as $\rm D_nH_m$) $n\mu_{\rm D} + m\mu_{\rm H} \leqslant H_{\rm f}(\rm D_nH_m)$, where D and H represent the dopant and host elements respectively.

As an example, we will describe the details of calculations for the case of a substitutional Ge impurity on a Ga site ($\rm Ge_{Ga}$). The formation energies and the charge transition levels for the other defects under consideration can be obtained in a similar way, using the values given here[5]. The calculated enthalpy of formation for GaTe compound is $H_{\rm f}$(GaTe) = −0.72 eV, therefore the μs must satisfy: $\mu_{\rm Ga} + \mu_{\rm Te} = -0.72$ eV and $\mu_{\rm i} \leqslant 0$ (i = Ga, Te, Ge). Since Ge can form a secondary phase with Te, with calculated $H_{\rm f}$(GeTe) = −0.14 eV, the maximum achievable value of the chemical potentials are further limited by the condition: $\mu_{\rm Ge} + \mu_{\rm Te} \leqslant -0.14$ eV. Under Ga-rich growth conditions ($\mu_{\rm Ga} = 0$, $\mu_{\rm Te} = -0.72$ eV) this gives $\mu_{\rm Ge} \leqslant -0.14 + 0.72 = 0.58$ eV. However, in order to avoid precipitations of Ge, we have to impose $\mu_{\rm Ge} \leqslant 0$. Under Te-rich conditions ($\mu_{\rm Ga} = -0.72$ eV, $\mu_{\rm Te} = 0$) on the other hand, $\mu_{\rm Ge}$ is reduced to −0.14 eV. Using equations (1) and (2), the formation energy of $\rm Ge_{Ga}$ in the neutral charge state is $\Delta H_{\rm f}(\rm Ge_{Ga}) = 1.18$ eV $+ \mu_{\rm Ga} - \mu_{\rm Ge}$. Under Ga-rich conditions ($\mu_{\rm Ga} = 0$, $\mu_{\rm Te} = -0.72$ eV and $\mu_{\rm Ge} = 0$) this gives $\Delta H_{\rm f}(\rm Ge_{Ga}) = 1.26$ eV, whereas under Te-rich conditions $\Delta H_{\rm f}(\rm Ge_{Ga})$ decreases to 0.60 eV. This is because under Te-rich (Ga-poor) conditions, Ga vacancies are more likely to appear making it easy for Ge atoms to occupy these vacancies. In the case of the charged defects, the formation energy also depends on the Fermi level, because in order to ionize the defect, electrons must be taken from or added to the electron reservoir with energy $E_{\rm F}$. The donor transition levels for $\rm Ge_{Ga}$ were calculated using equation (3): $\varepsilon(+/0) = 0.01$ eV and $\varepsilon(+2/+) = 0.75$ eV.

Figure 8 shows the calculated formation energies as a function of $E_{\rm F}$ for different defects. For $V_{\rm Ga}$ we find two acceptor levels $\varepsilon(0/-1)$ and $\varepsilon(-1/-2)$ in the band gap at 0.13 eV and 0.83 eV above the VBM, respectively. The latter is in very good agreement with the experimental results reported in [32, 33]. $V_{\rm Te}$ appears to be in the neutral charge state for almost all values of $E_{\rm F}$ across the band gap. Nevertheless, it introduces a deep donor level at 0.03 eV above the VBM. Furthermore, our calculations (not shown in the figure) show that the donor level $\varepsilon(+2/+1)$ is slightly higher in energy than $\varepsilon(+1/0)$, meaning that $V_{\rm Te}$ is a negative-U center, with an unstable +1 charge state. The substitutional defect $\rm Sn_{Ga}$ behaves similarly to $\rm Ge_{Ga}$, which was described in detail in the previous paragraph. The deep donor levels $\varepsilon(+2/+1)$ and $\varepsilon(+1/0)$ associated with $\rm Sn_{Ga}$ are located at 0.06 and 0.78 eV above the VBM.

From figure 8 we observe that the defect formation energies are quite sensitive to the growth conditions. First let us look at the intrinsic defects $V_{\rm Ga}$ and $V_{\rm Te}$. At the Te-rich limit, the formation energy of $V_{\rm Ga}$ is always less compared to $V_{\rm Te}$, indicating that Ga vacancies are more likely to appear during the Te-rich growth process. However, at the Ga-rich limit, we find that the formation energy of $V_{\rm Ga}$ relative to $V_{\rm Te}$ depends on the position of the Fermi level. If $E_{\rm F}$ is closer to the VBM (p-type material) the Te vacancy will be the dominant intrinsic defect, whereas if $E_{\rm F}$ is above the midgap (n-type material), the acceptor $V_{\rm Ga}$ will dominate over the donor $V_{\rm Te}$.

[5] The calculated formation energies $\Delta E(\alpha, q)$ using equation (2) are: $\Delta E(V_{\rm Te}, 0) = 2.17$ eV, $\Delta E(V_{\rm Te}, +1) = 2.15$ eV, $\Delta E(V_{\rm Te}, +2) = 2.12$ eV, $\Delta E(\rm Ge_{Ga}, 0) = 1.18$ eV, $\Delta E(\rm Ge_{Ga}, +1) = 0.43$ eV, $\Delta E(\rm Ge_{Ga}, +2) = 0.42$ eV, $\Delta E(\rm Sn_{Ga}, 0) = 1.02$ eV, $\Delta E(\rm Sn_{Ga}, +1) = 0.24$ eV, $\Delta E(\rm Sn_{Ga}, +2) = 0.18$ eV. The calculated enthalpies of formation are $H_{\rm f}$(GeTe) = −0.14 eV and $H_{\rm f}$(SnTe) = −0.61 eV.

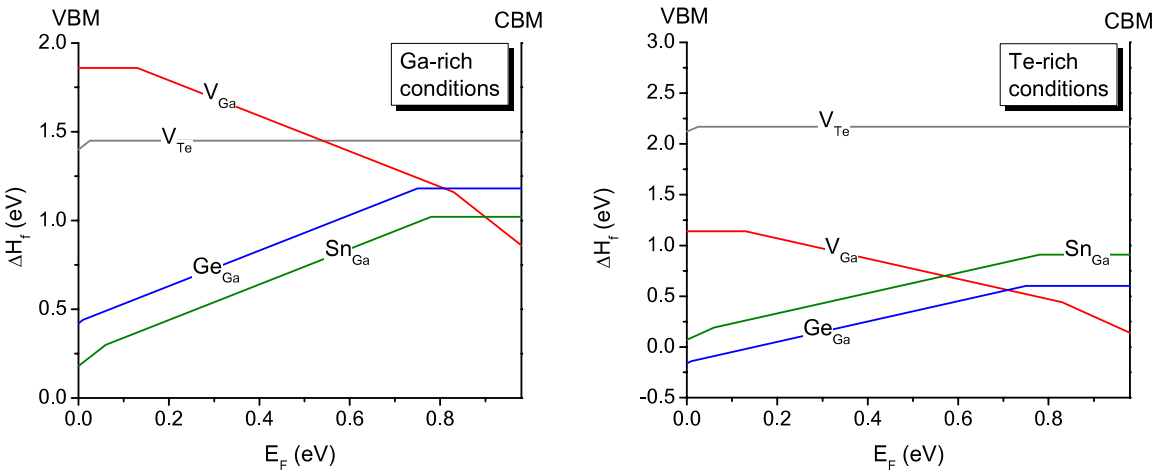

Figure 8. Calculated defect formation energies in GaTe as a function of Fermi energy, under Ga-rich and Te-rich conditions. The slope of the energy lines indicates the charge state of the defect and the value of E_F where the slope changes, represents the charge transition level.

We observe that the growth conditions also influence the solubility of Sn relative to the solubility of Ge. Under Ga-rich conditions it is easier to incorporate Sn in GaTe, whereas at the Te-rich limit Ge becomes more soluble than Sn. This is because the Sn–Te bond being stronger than the Ge–Te bond (H_f(SnTe) $= -0.61$ eV and H_f(GeTe) $= -0.14$ eV), it will be more likely for Sn to form secondary phases with the Te atoms, during the Te-rich growth process. In order to avoid this, we have to decrease the atomic chemical potential of the Sn, which in turn, increases the defect formation energy.

4. Summary

In summary, we have performed electronic structure calculations in pure and defect containing GaTe to understand the nature of local bondings and how they effect the overall band structure of pure GaTe and the defect states. The results obtained for the pure system indicate that it is a direct gap semiconductor. As in other III–VI semiconductors containing Ga–Ga dimers, the presence of these dimers and the interaction of the dimer states with Te p states lead to the formation of the band gap. Our results obtained without SOI agrees with previous works [6, 8]. In contrast to the suggestion made by Sanchez-Royo *et al* we do not find the SOI to be important in GaTe; the shifts in the energy levels near the VBM and CBM are ∼0.1 eV rather than ∼0.8 eV. To investigate the nature of various defects in GaTe, we constructed large supercell models (192 atoms). We find that a Ga vacancy introduces a deep defect state in the band gap region at ∼0.78 (∼0.82 eV) above the VBM of the defect containing (defect-free) system, at the Γ-point. The charge density associated with this defect level is strongly localized around the vacancy's NN Ga atom. The energy of the Ga vacancy induced defect band is in quite good agreement with the experimental observation [32, 33]. A Te vacancy introduces two single particle states near the CBM and a resonant state just below E_f. Charge densities associated with the gap states reveal the localized character for these bands. Ge and Sn substitutional impurities behave almost identically in the GaTe host, introducing a deep donor state in the band gap region.

Our calculations show that the defect formation energies depend not only on the charge state of the defect but also on the growth conditions (Ge-rich or Te-rich). In the case of n-type samples, however, V_{Ga} is always the dominant intrinsic acceptor, which can compensate the intentional donors. The calculated acceptor level $\varepsilon(-1/-2) = 0.83$ eV above the VBM is in good agreement with the experiment [32, 33]. We find that V_{Te} is a negative-U center with a deep $\varepsilon(+2/0)$ donor transition level located at 0.03 eV above the VBM. Our results also indicate that as the growth conditions change from Ga-rich to Te-rich, the solubilities of Sn and Ge interchange relative to each other. Both, Ge_{Ga} and Sn_{Ga}, are deep donors with the $\varepsilon(+2/+1)$ level located at 0.01 and 0.06 eV above the VBM and $\varepsilon(+1/0)$ level located at 0.75 and 0.78 eV above the VBM.

Acknowledgments

The work was partially supported by the department of Physics and Astronomy at Michigan State University (TA to Zsolt Rak) and a subcontract to MSU from the EIC Laboratories. One of the authors (KCM) acknowledges partial financial support by the Air Force under contract No. FA86540-06-M-541. Calculations were performed at the High Performance Computing Center at Michigan State University.

References

[1] Dmitriev V G, Gurzadyhan G G and Nikogosyan D N 1999 *Handbook of Nonlinear Optical Crystals* (New York: Springer) p 166
[2] Eckhoff W C, Putnam R S, Wang S, Curl R F and Tittel F K 1996 *Appl. Phys.* A **63** 437
[3] Hernández M A, Sánchez J F, Andrés M V, Segura A and Muñoz V 1993 *Opt. Pura Apl.* **26** 152
[4] Pearson W B 1964 *Acta Crystallogr.* **17** 1
[5] Julien-Pouzol M, Jaulmes S, Guittard M and Alapini F 1979 *Acta Crystallogr.* B **35** 2848

[6] Yamamoto A, Syouji A and Goto T 2001 *Phys. Rev.* B **64** 035210
[7] Irwin J C, Clayman P B and Mead D G 1979 *Phys. Rev.* B **19** 2099
[8] Sanchez-Royo J F, Pellicer-Porres J, Segura A, Munoz-Sanjose V, Tobias G, Ordejon P, Canadell E and Huttel Y 2002 *Phys. Rev.* B **65** 115201
[9] Fischer G and Brebner J L 1962 *J. Phys. Chem. Solids* **23** 1363
[10] Brebner J L, Fischer G and Mooser E 1962 *J. Phys. Chem. Solids* **23** 1417
[11] Consadori F and Brebner J L 1973 *Solid State Commun.* **12** 179
[12] Camassel J, Merle P, Mathieu H and Gouskov A 1979 *Phys. Rev.* B **19** 1060
[13] Camassel J, Merle P and Mathieu H 1980 *Physica* B **99** 309
[14] Schwarz U, Syassen K and Kniep R 1995 *J. Alloys Compounds* **224** 212
[15] Pellicer-Porres J, Manjon F J, Segura A and Munoz V 1999 *Phys. Rev.* B **60** 8871
[16] Pellicer-Porres J, Manjon F J, Segura A and Munoz V 2000 *Phys. Rev.* B **61** 125
[17] Efeoğlu H, Karacali T, Abay B and Yoğurtçu Y K 2004 *Semicond. Sci. Technol.* **19** 523
[18] Schultz P A 2006 *Phys. Rev. Lett.* **96** 246401
[19] Blöchl P E 1994 *Phys. Rev.* B **50** 17953
Kresse G and Joubert D 1999 *Phys. Rev.* B **59** 1758
[20] Kresse G and Hafner J 1993 *Phys. Rev.* B **47** 558
Kresse G and Hafner J 1994 *Phys. Rev.* B **49** 14251
Kresse G and Furthmüller J 1996 *Phys. Rev.* B **54** 11169
Kresse G and Furthmüller J 1996 *Comput. Mater. Sci.* **6** 15
[21] Perdew J P, Burke K and Ernzerhof M 1996 *Phys. Rev. Lett.* **77** 3865
[22] Press W H, Flannery B P, Teukolsky S A and Vetterling W T 1992 *Numerical Recipes* (New York: Cambridge University Press)
[23] Monkhorst H J and Pack J D 1976 *Phys. Rev.* B **13** 5188
[24] Nieminen R M 2007 *Theory of Defects in Semiconductors* ed D A Drabold and S Estreicher (Berlin: Springer)
[25] Singh D J 1994 *Planewaves, Pseudopotentials, and the LAPW Method* (Boston, MA: Kluwer–Academic)
[26] Blaha P, Schwartz K, Madsen G K H, Kvasnicka D and Luitz J 2001 *WIEN2K, An Augmented Plane Wave + Local Orbitals Program for Calculating Crystal Properties* ed K Schwarz (Wien: Technical Universitat Wien)
[27] Williams R H, McGovern I T, Murray R B and Howells M 1976 *Phys. Status Solidi* b **73** 307
[28] Hoang K 2007 Atomic and electronic structures of novel ternary and quaternary narrow band-gap semiconductors *Dissertation for the Degree of PhD* Michigan State University, USA
[29] Camara M O D, Mauger A and Devos I 2002 *Phys. Rev.* B **65** 125206
[30] Madelung O 2004 *Semiconductors: Data Handbook* (Berlin: Springer) p 527
[31] Aulbur W G, Jonsson L and Wilkins J W 2000 *Solid State Physics* vol 54 (Orlando, FL: Academic)
[32] Shigetomi S, Ikari T and Nakashima H 1998 *Japan. J. Appl. Phys.* **37** 3282
[33] Manfredotti C, Murri R, Rizzo A, Vasanelli L and Micocci G 2006 *Phys. Status Solidi* a **29** 475
[34] Rak Zs, Mahanti S D, Mandal K C and Fernelius N C 2007 *Proc. MRS* p 0994-F03-10
[35] Zhang S B and Northrup E 1991 *Phys. Rev. Lett.* **67** 2339
[36] Zhang S B 2002 *J. Phys.: Condens. Matter* **14** 881
[37] Wei S H and Zhang S B 2002 *Phys. Rev.* B **66** 155211